Alzheimer's & Dementia: Translational Research & Clinical Interventions 5 (2019) 610-617

Featured Article

Vascular retinal biomarkers improves the detection of the likely cerebral amyloid status from hyperspectral retinal images

Sayed Mehran Sharafi[a], Jean-Philippe Sylvestre[b], Claudia Chevrefils[b], Jean-Paul Soucy[c], Sylvain Beaulieu[d], Tharick A. Pascoal[e], Jean Daniel Arbour[f], Marc-André Rhéaume[f], Alain Robillard[g], Céline Chayer[g], Pedro Rosa-Neto[h], Sulantha S. Mathotaarachchi[h], Ziad S. Nasreddine[i], Serge Gauthier[j], Frédéric Lesage[a,k,*]

[a]*Genie Electrique, Polytechnique Montreal, Montreal, Quebec, Canada*
[b]*Optina Diagnostics, Montreal, Quebec, Canada*
[c]*Montreal Neurological Institute, McGill University, Montreal, Quebec, Canada*
[d]*Département de médecine nucléaire, Hôpital Maisonneuve-Rosemont, Montreal, Quebec, Canada*
[e]*Translational Neuroimaging Laboratory, McGill Centre for Studies in Aging, Douglas Mental Health University Institute, Montreal, Quebec, Canada*
[f]*Clinique ophtalmologique 2121, Montreal, Quebec, Canada*
[g]*Département de psychiatrie, Hôpital Maisonneuve-Rosemont, Montreal, Quebec, Canada*
[h]*Translational Neuroimaging Laboratory, McGill Centre for Studies in Aging Douglas Mental Health University Institute, Montreal, Quebec, Canada*
[i]*MoCA Clinic and Institute, Greenfield Park, Quebec, Canada*
[j]*Alzheimer's Disease Research Unit, The McGill University Research Centre for Studies in Aging, Montreal, Quebec, Canada*
[k]*Research Center, Montreal Heart Institute, Montreal, Quebec, Canada*

Abstract

Introduction: This study investigates the relationship between retinal image features and β-amyloid (Aβ) burden in the brain with the aim of developing a noninvasive method to predict the deposition of Aβ in the brain of patients with Alzheimer's disease.

Methods: Retinal images from 20 cognitively impaired and 26 cognitively unimpaired cases were acquired (3 images per subject) using a hyperspectral retinal camera. The cerebral amyloid status was determined from binary reads by a panel of 3 expert raters on ^{18}F-florbetaben positron-emission tomography (PET) studies. Image features from the hyperspectral retinal images were calculated, including vessels tortuosity and diameter and spatial-spectral texture measures in different retinal anatomical regions.

Results: Retinal venules of amyloid-positive subjects (Aβ+) showed a higher mean tortuosity compared with the amyloid-negative (Aβ−) subjects. Arteriolar diameter of Aβ+ subjects was found to be higher than the Aβ− subjects in a zone adjacent to the optical nerve head. Furthermore, a significant difference between texture measures built over retinal arterioles and their adjacent regions were observed in Aβ+ subjects when compared with the Aβ−. A classifier was trained to automatically discriminate subjects combining the extracted features. The classifier could discern Aβ+ subjects from Aβ− subjects with an accuracy of 85%.

Discussion: Significant differences in texture measures were observed in the spectral range 450 to 550 nm which is known as the spectral region known to be affected by scattering from amyloid aggregates in the retina. This study suggests that the inclusion of metrics related to the retinal vasculature and tissue-related textures extracted from vessels and surrounding regions could improve the discrimination performance of the cerebral amyloid status.

J.-P.S. and C.C. are employees of Optina. J.D.A. has partial ownership in Optina.

*Corresponding author. Tel.: 1 514 340-4711 x 7542; Fax: 1 514 340-4611.

E-mail address: frederic.lesage@polymtl.ca or image.liom@polymtl.ca (F.L.)

https://doi.org/10.1016/j.trci.2019.09.006

Keywords: Multispectral fundus imaging; Alzheimer; Beta amyloid; Retina; Image processing; Machine learning

1. Introduction

Alzheimer's disease (AD) is a slowly evolving neurodegenerative disorder characterized by cognitive loss that ultimately leads to a state of major cognitive impairment. It is the most common cause of major cognitive impairment, affecting millions worldwide. The hallmark histopathological anomalies of AD result from the progressive accumulation of extracellular β-amyloid (Aβ) plaques composed of amyloid precursor protein fragments, Aβ peptides, and the intracellular tau tangles, composed of fibrils of hyper phosphorylated tau protein [1]. Pathological changes can occur up to 20 years earlier than the onset of cognitive decline, and brain degeneration has already spread widely by the time the cognitive decline becomes apparent. The National Institute of Aging and the Alzheimer's Association, as well as of the International Working Group on AD recently proposed a research framework based on a set of validated biomarkers linked among others to both types of anomalies that are proxies for AD to define AD in living people [2].

Positron-emission tomography (PET) imaging with Aβ ligands is the standard noninvasive method for *in vivo* detection of Aβ plaques in the brain. They can indicate the presence, distribution, and quantity of Aβ in the brain. Although the cerebral amyloid status on its own is not specific to AD, there is growing evidence that amyloid PET helps confirm or rule out the diagnosis, and can be useful for the optimization of patient management [3–5]. However, PET with Aβ ligands is an expensive technique of limited accessibility and costs and practical limitations restrain its use for population screening. There has also been significant progress in the area of cerebrospinal fluid biomarkers for AD. To date, decreased $A\beta_{42}$ or $A\beta_{42}/A\beta_{40}$ ratio and high levels of p-Tau are the most accurate, reproducible, and informative cerebrospinal fluid biomarkers for AD [6,7]. However, these require lumbar puncture and standardization has proven to be complex.

The retina is an extension of the central nervous system (CNS) and represents the only part of the CNS which is noninvasively accessible for imaging by optical means. The eye therefore has been therefore suggested as a window to the brain offering a unique site to measure biomarkers for neurodegenerative diseases [8,9].

Spectral domain optical coherence tomography has allowed 3-dimentional observation of histological details of the retinal layers and optic nerve with high resolution (4 μm axial resolution). Spectral domain optical coherence tomography is currently being applied to various CNS neurodegenerative diseases [10] by measuring retinal nerve fibre layer loss and has been demonstrated to show nerve fiber anomalies in AD [11–14]. However, the method may lack specificity, as nerve fiber alterations are also observed in glaucoma, MCI [13], and Parkinson's disease [15,16].

It was reported in the literature that Aβ plaques accumulate in the retina of AD mouse models [17–21], an accumulation also observed in the retina of AD human subjects post mortem [18] and *in vivo* [22,23].

Optical fluorescence imaging of the retina, with the fluorescent label curcumin, which binds to Aβ plaques with high affinity [24,25], has been proposed as a simple procedure to detect Aβ plaques [18] and has recently been tested *in vivo* in AD subjects [22,23]. However, the latter study involved two visits by volunteers for retinal fluorescence imaging with the oral administration of a curcumin supplement between appointments and blood testing to confirm curcumin uptake.

Separately, an infrared laser confocal quasi-elastic light scattering procedure and the Fluorescent Ligand Eye Scanning technique [26] have been developed to detect amyloid-related pathology in the ocular lens. Aβ has been shown to accumulate in the retina and lens in patients with AD [26,27–29]. These methods, however, are limited to subjects who have not been operated for cataracts as the presence of the natural eye lens is required. This technique also involves the application of an extraneous fluorescent label.

Spectral changes were also reported in mice with AD relative to age-matched wild-type mice *ex vivo* [30] and *in vivo* [31] using label-free reflectance hyperspectral retinal images. A similar phenomenon was observed in human brain and retina tissue *ex vivo*. These results support the idea that hyperspectral retinal imaging could be used to identify amyloid-related signs of CNS AD deposition without extraneous labeling. Owing to the much higher interindividual variability of fundus reflectance in humans, however, direct translation to useful applications in humans of the described method, based exclusively on the spectral evaluation of the data sets, is unlikely when compared with a uniform mice cohort. This variability may overwhelm the effect of Aβ aggregates on the spectral signal. More advanced image analysis techniques than the direct spectral evaluation proposed by the authors will likely be required to isolate the spectral signature of amyloid in the human tissue.

Literature has also shown correlations between retinal vessels abnormalities and AD [8,11,32–35] suggesting a potential for retinal imaging to deliver new biomarkers of the disease. Among those, retinal vascular tortuosity (RVT) is caused by the natural capability of vessels to adapt to factors associated with certain diseases [36–40]. RVT has been studied as an indicator of blood pressure and cardiovascular diseases [41–43], diabetes, neuroretinal rim thinning [37], diabetic retinopathy, hypertensive retinopathy, retinopathy of prematurity, facioscapulohumeral muscular dystrophy, and Coats diseases [44,45]. Recent

studies have further shown a relationship between RVT and AD [33,35,46,47].

A simple, noninvasive, and accessible technique to establish the presence or absence of cerebral amyloid plaques by looking at the retina has recently been developed by Optina Diagnostics. It uses the Metabolic Hyperspectral Retinal Camera (MHRC), a system that permits the acquisition of a series of retinal images obtained at specific wavelengths covering the visible and near infrared spectrum in combination with a proprietary classifier using spatial and spectral texture features obtained with the MHRC to determine the likely amyloid status of the brain. This approach does not aim to visualize directly amyloid deposits in the retina but rather to determine a likely amyloid status based on sets of image features highly correlated with the cerebral amyloid status.

The purpose of this study was to derive retinal vascular metrics from the hyperspectral retinal images and to evaluate their capability to discriminate subjects based on their cerebral PET amyloid status, on their own and in combination with texture metrics extracted from the hyperspectral retinal images. To that end, RVT and retinal vessels diameter were evaluated from images of a hyperspectral fundus camera. They were combined with spatial/spectral texture measures, taken over and around vessels to identify discriminating features. After dimensional reduction, the predictive power of the measures was evaluated using a Support Vector Machine (SVM) classifier trained using the final set of features to discriminate between Aβ-positives and Aβ-negative subjects as define by PET scanning.

2. Methods

2.1. Subjects

All procedures were approved by the ethics committees of Polytechnique Montreal, McGill University, Hopital Maisonneuve-Rosemont and Véritas IRB. Subjects were aged between 60 and 85 years and had no retinal diseases or significant ocular media opacity, as determined by an ophthalmological evaluation. The studied cohort (n = 46) included 20 cognitively impaired subjects (values outside the normal range for the Mini–Mental State Examination and/or the Montreal Cognitive Assessment) and 26 control cases with unimpaired cognition. After PET amyloid imaging, 7 of 20 cognitively impaired cases were identified as amyloid negative, whereas 3 of the 26 cognitively normal subjects were amyloid positive.

2.2. Hyperspectral retinal imaging

Pupils were dilated (>6 mm) using 1% w/v tropicamide and 2.5% w/v phenylephrine before the ophthalmological evaluation and retinal imaging. Retinal images were acquired using an MHRC developed by Optina Diagnostics [48,49]. The MHRC is based on a custom-built mydriatic fundus camera incorporating a tunable light source, able to transmit safe light levels within a spectral range covering the visible to the near-infrared region of the spectrum within a series of narrow bandwidths (<3 nm). A schematic of the MHRC is shown in Fig. 1. Images of the retina on a field of view of ~30° were sequentially obtained for different monochromatic illumination wavelengths to build a cube of 91 images obtained in the spectral range of 450 to 900 nm in steps of 5 nm in approximately 1 second. The images were normalized as previously described to correct for the response of the instrument and spatially registered to correct wavelength-dependent optical deformations (scaling) and eye movements (translation and rotation) that may occur during the acquisition.

2.3. Amyloid PET status determination

Amyloid imaging was performed using ^{18}F-florbetaben at a dose of 300 MBq (approx. 8.0 mCi) ± 20% on a General

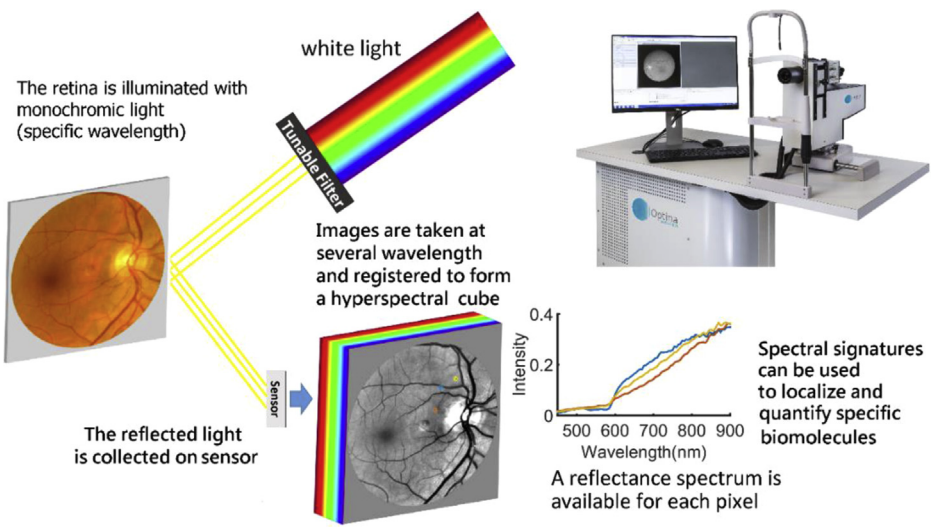

Fig. 1. Schematic of the metabolic hyperspectral retinal camera used for acquiring the images.

Electric PET/CT Discovery ST16. A very low-dose CT pilot study was performed to permit optimal positioning of the acquisition field centered on the brain. A low-dose computed tomography acquisition was performed initially to permit attenuation correction (40 mAs, 140 kvP. Pitch 3). PET acquisition was performed in 3D mode over a period of 20 minutes. Ordered subset expectation maximization iterative reconstruction (2 subsets, 10 iterations) was performed subsequently, with correction for attenuation by low-dose computed tomography. The reconstruction also includes the standard corrections for scattered photons and random detection. The cerebral amyloid status was determined from binary reads by a panel of 3 expert readers with experience in reporting such studies. Each reader evaluated independently the amyloid PET scans for all the participants of the study and an in-person meeting was organized with all three readers to review cases where readings were discordant to rule on a final amyloid status for each participant.

2.4. Retinal data processing

2.4.1. Vessels segmentation

All vessels with a diameter larger than 3 pixels (approximately 25 μm) were automatically segmented and classified as arterioles and venules. Results were corrected for any misclassification using a graphical user interface built for this task.

2.4.2. Tortuosity measurement

Vessels segments between bifurcations were extracted and thinned to their skeleton, then tortuosity of each vessel segment was computed by taking the integral of the square derivative of curvature divided by the length of a curve [50] (a comprehensive review on RVT metrics is available in the study by Abdalla et al [51]). For each of the images, average RVT values of arterioles and venules were calculated separately for all segmented vessels described previously, except for vasculature located inside the optical nerve head (ONH) which was masked and excluded from the RVT measurements. Aβ+ and Aβ− subjects were compared based on average arterioles tortuosity and venules tortuosity separately. Fig. 2 A illustrates sample outputs of the software developed for vessels' tortuosity measurement with a curvature map of a vessel segment.

2.4.3. Diameter measurements

For each vessel segment located between two bifurcations, one-third of the centerline pixels were randomly chosen. The diameter of the vessel segment was calculated as the average of the length of the shortest paths passing through the selected centerline pixels. Vessel diameters were calculated for three different retinal zones (Fig. 2 B) by taking the maximum of the vessels' diameters within the associated zone.

2.4.4. Image analysis

Image features were built using standard image texture measures that included contrast, correlation, energy, homogeneity, standard deviation, range, and entropy [52]. The textures were calculated along the spectral dimension of the hyperspectral imaging cube and along a combination of spectral and spatial dimensions. In addition to the full range of the available spectrum (i.e. 450–900 nm), different bands in between were separately investigated for texture measurements following observations of maximal spectral changes in specific bands. The measures were calculated for different vascular anatomical areas of the retina including arterioles, venules, and regions around arterioles and venules (separately).

2.4.5. Feature selection and classification

An initial set of features included vessels' tortuosity, diameter, AVR, and texture measures extracted from arterioles and venules and adjacent regions (including about 83 μm away from the vessel's border). After a sequential feature selection, 8 features with highest validation criterion were selected. The validation criterion was evaluated through a 10-fold cross-validation of the initial set of features by repeatedly fitting a multivariate normal density

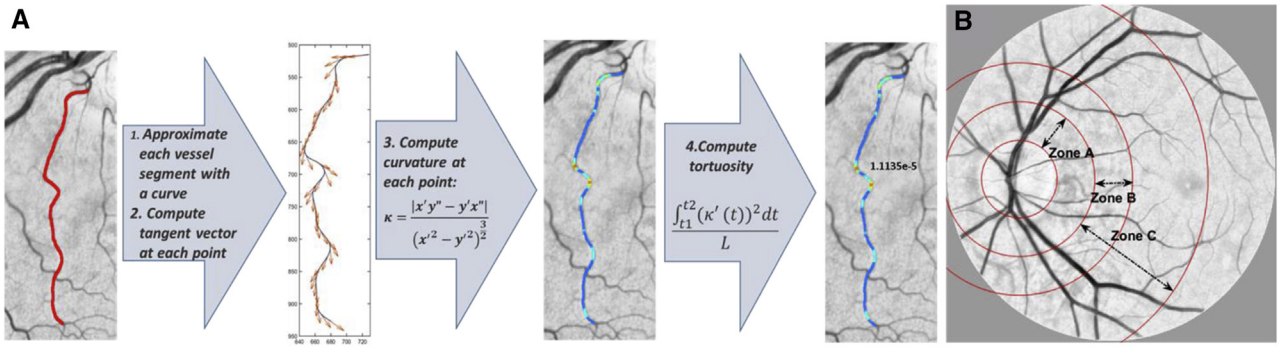

Fig. 2. (A) Tortuosity measurement steps of a sample vessel segment. (B) Different zones of retina: zone A (region from 0 to 0.5 ONH diameters away from the ONH margin), zone B (region from 0.5 to 1 ONH diameters away from the ONH margin), and zone C (region from 0.5 to 2 ONH diameters away from the ONH margin).

Table 1
Eight features chosen by sequential feature selection

Feature code	Feature name	Anatomical region	Band(nm)	Direction	*P* value
F1	Tortuosity	Venules	-	-	$1.6e^{-6}$
F2	Diameter	Arterioles—zone A	-	-	.0104
F3	Contrast (texture)	Arterioles and around	450–550	Spectral	$1.05e^{-6}$
F4	Energy (texture)	Arterioles and around	450–550	Spectral	$9.6e^{-7}$
F5	Energy (texture)	Arterioles	700–900	Spectral	.0056
F6	Contrast (texture)	Arterioles and around	450–550	Spatial-spectral	$7.4e^{-5}$
F7	Correlation (texture)	Arterioles and around	450–550	Spatial-spectral	.0160
F8	Homogeneity (texture)	Arterioles and around	450–550	Spatial-spectral	$2.9e^{-5}$

NOTE. Anatomical regions, bands, directions in which features were extracted and Bonferroni-corrected *P* values are shown.

function to each group of data (i.e. Aβ+ and Aβ−), with different training and testing subsets. Table 1 summarizes the selected features and their attributes. Although texture measures are dependent features, we corrected *P* values based on Bonferroni correction to illustrate the minimum *P* value that could be considered for each of the features. Following principal component analysis of the features in Table 1, an SVM classifier with linear kernel was trained to discern Aβ+ subjects from Aβ− subjects.

3. Results

Retinal venules of the PET amyloid-positive subjects showed a higher mean tortuosity compared with the amyloid-negative subjects ($P < 1.6e\text{-}6$). In addition, significant difference was observed between arterioles' tortuosity of Aβ+ and Aβ− subjects ($P < .002$). Moreover, mean arterioles' diameters in zone A ($P < .011$) and zone C ($P < .02$) showed a significant difference between the two groups of subjects. Different textures measures of arterioles and adjacent regions also showed significant differences in Aβ+ retinal images compared with Aβ−. To provide the full distribution, Fig. 3 illustrates the data points, mean, SEM (light gray) and standard deviations (dark gray) and associated *P* values of each feature identified through the selection process.

For automatic discrimination of Aβ+ from Aβ− subjects, features F1 to F8 were used to train an SVM classifier with linear kernel. Ten-fold cross-validation was conducted to evaluate classification loss of the classifier (from observations not used for training). Fig. 4 A shows how classification loss of this classifier changes by stepwise appending the principal components of the features F1 to F8. The distribution of classification loss values was evaluated by repetitive execution of 10-fold cross-validation in each step. The smallest cross-validation loss is associated with 7th principal component (0.14 ± 0.005).

Finally, to investigate the benefit of combining different types of features, that is, vasculature features and texture measures in improving the accuracy of discrimination between Aβ+ and Aβ− subjects, we evaluated the accuracy of the classification using texture measures (F3 to F8) and

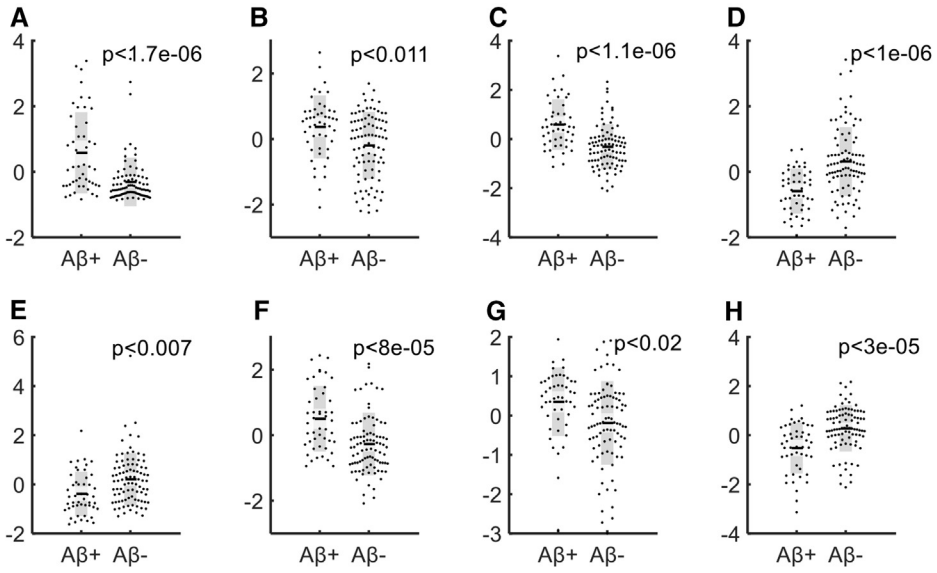

Fig. 3. Difference between β-amyloid-positive and β-amyloid-negative data sets corresponding to features F1 (A) to F8 (H)—Data points are shown as normalized values.

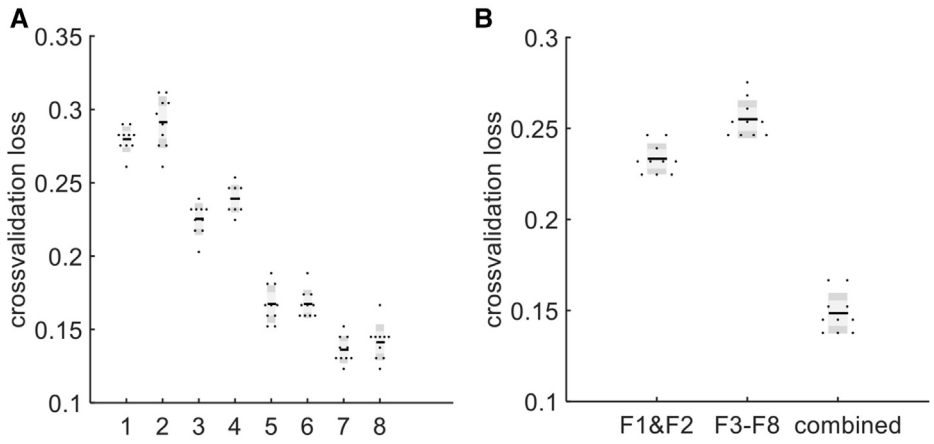

Fig. 4. (A) SVM classification loss using principal components 1 to 8 inclusively; (B) comparison of classification losses when using different types of features.

vasculature features (F1 and F2) separately. Fig. 4 B compares classification loss when using vasculature (F1 and F2), textures (F3 to F8), and combined features (7 principal components of F1 to F8). One can observe that lowest classification loss (0.14 ± 0.005) is obtained when using a combined approach confirming the added information content of hyperspectral imaging.

Finally, Table 2 shows a comparison among classifications' accuracy when using different types of features. Sensitivity, specificity, positive predictive value and negative predictive value were obtained using a 10-fold cross validation.

4. Discussion

In this work, we aimed to establish a correlation between retinal image features related to the vasculature with cerebral Aβ deposition in the brain. The study was conducted using images taken by a novel hyperspectral imaging platform in a group of cognitively impaired and cognitively unimpaired subjects with known cerebral amyloid status determined by amyloid PET.

One of the findings was that both retinal arterioles and venules tortuosity were significantly higher in Aβ+ subjects than in Aβ− subjects ($P < .002$, $P < 1.6e\text{-}6$). This supports recent findings on the correlation between RVT and cognitive impairment [35,46,53] as well as RVT and amyloid deposition in the brain [33]. In the study by Cheung et al [54], both arteriolar and venular tortuosity are reported to be increased in AD, whereas in the study by Cheung et al [41], both arteriolar and venular tortuosity are reported to be inversely proportional to aging (between 60 and 80 yrs). Considering the latter finding along with the studies supporting the increase of retinal vessels' tortuosity in patients with AD shows the importance of retinal vessels' tortuosity as a potential biomarker of AD among elderly subjects. Here, we quantitatively observed that not only the vessels' tortuosity, but also arteriole diameters in zone A ($P < .02$) and texture measures taken over retinal arterioles and adjacent areas ($P < 1e\text{-}6$) of Aβ+ subjects are significantly different from retinal images of Aβ− subjects. Significant differences in texture measures were observed in the spectral range 450 to 550 nm which is known as the spectral region most likely to be affected by scattering from amyloid aggregates in the retina. Also, we observed significant difference in texture measures in the spectral range 700 to 900 nm ($P < .0008$) which is the spectral region least likely to be affected by the transmission of the anterior segment of the eye.

Despite significant difference between the groups, the important overlap between Aβ+ and Aβ− subjects (Fig. 3) means that individual image features cannot achieve good separation of the two groups. We therefore used a combination of vasculature features and texture measures to classify Aβ+ and Aβ− subjects using an SVM classifier. Results showed that a classifier trained with vasculature measures alone, could discriminate Aβ+ from Aβ− subjects with an accuracy of 76%; however, combining vascular

Table 2
Comparing classification performance based on features used

Features used	Sensitivity	Specificity	PPV	NPV	Accuracy
Vasculature features (F1 and F2)	0.74 ± 0.019	0.77 ± 0.006	0.49 ± 0.018	0.91 ± 0.007	0.76 ± 0.008
Texture measures (F3 to F8)	0.68 ± 0.022	0.76 ± 0.007	0.50 ± 0.019	0.87 ± 0.012	0.74 ± 0.010
Combined (7 PCs of F1 to F8)	0.82 ± 0.022	0.86 ± 0.011	0.73 ± 0.025	0.91 ± 0.011	0.85 ± 0.013

NOTE. Performance values were evaluated using different gold standards: cognitive tests (Cog.) and amyloid status (Aβ).
Abbreviations: PPV, positive predictive value; NPV, negative predictive value.

metrics with a set of spatial-spectral texture metrics resulted in a more accurate prediction of cerebral amyloid status with a classification loss of 0.14 ± 0.005 and accuracy of 85%. It should be noted that based on the method, type of textures, and the parameters used, the classification performance of texture features alone could be further optimized. For example, the proprietary method developed by Optina Diagnostics [55] achieved higher accuracy than the texture-based classification results shown in the second row of Table 2.

Overall, this study suggests that the inclusion of metrics related to the retinal vasculature in a classifier built from features extracted from hyperspectral retinal images could improve the discrimination performance of the cerebral amyloid status.

Acknowledgment

This work was financed by the Consortium Québécois sur la Découverte du Médicament—CQDM.

RESEARCH IN CONTEXT

1. Systematic review: Limitation of the current diagnostics of Alzheimer's disease based on PET imaging with Aβ ligands and measuring levels of p-Tau in cerebrospinal fluid were stated. Moreover, methods that rely on investigation of eye biomarkers using spectral domain optical coherence tomography, optical fluorescence imaging, and fluorescent ligand eye scanning were reviewed and their limitations for popular screening were stated.
2. Interpretation: In this work, using a novel hyperspectral retinal imaging device, we showed that correlation exists between retinal vasculature characteristics and image textures extracted from retinal arterioles and venules and surrounding regions with the cerebral Aβ deposition in the brain. A classifier built from features extracted from hyperspectral retinal images could improve the discrimination performance of the cerebral amyloid status.
3. Future directions: Further work to explore serial monitoring of retinal images in correlation with disease time-course could help define a clinical scenario for fundus imaging in Alzheimer's disease.

References

[1] Masters CL, Bateman R, Blennow K, Rowe CC, Sperling RA, Cummings JL. Alzheimer's disease. Nat Rev Dis Primers 2015; 1:15056.

[2] Jack CR Jr, Bennett DA, Blennow K, Carrillo MC, Dunn B, Haeberlein SB, et al. NIA-AA research framework: toward a biological definition of Alzheimer's disease. Alzheimers Dement 2018; 14:535–62.

[3] Ceccaldi M, Jonveaux T, Verger A, Krolak-Salmon P, Houzard C, Godefroy O, et al. Added value of 18F-florbetaben amyloid PET in the diagnostic workup of most complex patients with dementia in France: a naturalistic study. Alzheimers Dement 2018;14:293–305.

[4] Grundman M, Johnson KA, Lu M, Siderowf A, Dell'Agnello G, Arora AK, et al. Effect of amyloid imaging on the diagnosis and management of patients with cognitive decline: impact of appropriate use criteria. Dement Geriatr Cogn Disord 2016;41:80–92.

[5] Rabinovici GD, Gatsonis C, Apgar C, Gareen IF, Hanna L, Hendrix J, et al. Impact of amyloid PET on patient management: early results from the ideas study. Alzheimers Dement 2017;13:P1474.

[6] Kuhlmann J, Andreasson U, Pannee J, Bjerke M, Portelius E, Leinenbach A, et al. CSF Aβ1-42–an excellent but complicated Alzheimer's biomarker–a route to standardisation. Clin Chim Acta 2017;467:27–33.

[7] Olsson B, Lautner R, Andreasson U, Öhrfelt A, Portelius E, Bjerke M, et al. CSF and blood biomarkers for the diagnosis of Alzheimer's disease: a systematic review and meta-analysis. Lancet Neurol 2016;15:673–84.

[8] Javaid FZ, Brenton J, Guo L, Cordeiro MF. Visual and ocular manifestations of Alzheimer's disease and their use as biomarkers for diagnosis and progression. Front Neurol 2016;7:55.

[9] Shah TM, Gupta SM, Chatterjee P, Campbell M, Martins RN. Beta-amyloid sequelae in the eye: a critical review on its diagnostic significance and clinical relevance in Alzheimer's disease. Mol Psychiatry 2017;22:353–63.

[10] Kesler A, Vakhapova V, Korczyn AD, Naftaliev E, Neudorfer M. Retinal thickness in patients with mild cognitive impairment and Alzheimer's disease. Clin Neurol Neurosurg 2011;113:523–6.

[11] Berisha F, Feke GT, Trempe CL, McMeel JW, Schepens CL. Retinal abnormalities in early Alzheimer's disease. Invest Opthalmol Vis Sci 2007;48:2285.

[12] Jindahra P, Hedges TR, Mendoza-Santiesteban CE, Plant GT. Optical coherence tomography of the retina: applications in neurology. Curr Opin Neurol 2010;23:16–23.

[13] Paquet C, Boissonnot M, Roger F, Dighiero P, Gil R, Hugon J. Abnormal retinal thickness in patients with mild cognitive impairment and Alzheimer's disease. Neurosci Lett 2007;420:97–9.

[14] Parisi V, Restuccia R, Fattapposta F, Mina C, Bucci MG, Pierelli F. Morphological and functional retinal impairment in Alzheimer's disease patients. Clin Neurophysiol 2001;112:1860–7.

[15] Jiménez-Jiménez FJ, Alonso-Navarro H, García-Martín E, Agúndez JAG. Cerebrospinal fluid biochemical studies in patients with Parkinson's disease: toward a potential search for biomarkers for this disease. Front Cell Neurosci 2014;8:369.

[16] Lee J-Y, Kim JM, Ahn J, Kim H-J, Jeon BS, Kim TW. Retinal nerve fiber layer thickness and visual hallucinations in Parkinson's Disease. Mov Disord 2014;29:61–7.

[17] Edwards MM, Rodríguez JJ, Gutierrez-Lanza R, Yates J, Verkhratsky A, Lutty GA. Retinal macroglia changes in a triple transgenic mouse model of Alzheimer's disease. Exp Eye Res 2014;127:252–60.

[18] Koronyo-Hamaoui M, Koronyo Y, Ljubimov AV, Miller CA, Ko MK, Black KL, et al. Identification of amyloid plaques in retinas from Alzheimer's patients and noninvasive in vivo optical imaging of retinal plaques in a mouse model. NeuroImage 2011;54:S204–17.

[19] Liu B, Rasool S, Yang Z, Glabe CG, Schreiber SS, Ge J, et al. Amyloid-peptide vaccinations reduce β-amyloid plaques but exacerbate vascular deposition and inflammation in the retina of Alzheimer's transgenic mice. Am J Pathol 2009;175:2099–110.

[20] Ning A, Cui J, To E, Ashe KH, Matsubara J. Amyloid-beta deposits lead to retinal degeneration in a mouse model of Alzheimer disease. Invest Ophthalmol Vis Sci 2008;49:5136–43.

[21] Perez SE, Lumayag S, Kovacs B, Mufson EJ, Xu S. Beta-amyloid deposition and functional impairment in the retina of the APPswe/

PS1DeltaE9 transgenic mouse model of Alzheimer's disease. Invest Ophthalmol Vis Sci 2009;50:793–800.
[22] Frost S, Kanagasingam Y, Macaulay L, Koronyo-Hamaoui M, Koronyo Y, Biggs D, et al. Retinal amyloid fluorescence imaging predicts cerebral amyloid burden and Alzheimer's disease. Alzheimers Dement 2014;10:P234–5.
[23] Koronyo Y, Biggs D, Barron E, Boyer DS, Pearlman JA, Au WJ, et al. Retinal amyloid pathology and proof-of-concept imaging trial in Alzheimer's disease. JCI Insight 2017;2:e93621.
[24] Garcia-Alloza M, Borrelli LA, Rozkalne A, Hyman BT, Bacskai BJ. Curcumin labels amyloid pathology in vivo, disrupts existing plaques, and partially restores distorted neurites in an Alzheimer mouse model. J Neurochem 2007;102:1095–104.
[25] Yang F, Lim GP, Begum AN, Ubeda OJ, Simmons MR, Ambegaokar SS, et al. Curcumin inhibits formation of amyloid beta oligomers and fibrils, binds plaques, and reduces amyloid in vivo. J Biol Chem 2005;280:5892–901.
[26] Kerbage C, Sadowsky CH, Tariot PN, Agronin M, Alva G, Turner FD, et al. Detection of amyloid β signature in the lens and its correlation in the brain to aid in the diagnosis of Alzheimer's disease. Am J Alzheimers Dis Other Demen 2015;30:738–45.
[27] Dentchev T, Milam AH, Lee VM-Y, Trojanowski JQ, Dunaief JL. Amyloid-beta is found in drusen from some age-related macular degeneration retinas, but not in drusen from normal retinas. Mol Vis 2003; 9:184–90.
[28] Goldstein LE, Muffat JA, Cherny RA, Moir RD, Ericsson MH, Huang X, et al. Cytosolic beta-amyloid deposition and supranuclear cataracts in lenses from people with Alzheimer's disease. Lancet 2003;361:1258–65.
[29] Johnson LV, Leitner WP, Rivest AJ, Staples MK, Radeke MJ, Anderson DH. The Alzheimer's A beta -peptide is deposited at sites of complement activation in pathologic deposits associated with aging and age-related macular degeneration. Proc Natl Acad Sci U S A 2002; 99:11830–5.
[30] More SS, Vince R. Hyperspectral imaging signatures detect amyloidopathy in Alzheimer's mouse retina well before onset of cognitive decline. ACS Chem Neurosci 2015;6:306–15.
[31] More SS, Beach JM, Vince R. Early detection of amyloidopathy in Alzheimer's mice by hyperspectral endoscopy. Invest Ophthalmol Vis Sci 2016;57:3231–8.
[32] Feke GT, Hyman BT, Stern RA, Pasquale LR. Retinal blood flow in mild cognitive impairment and Alzheimer's disease. Alzheimers Dement 2015;1:144–51.
[33] Frost S, Kanagasingam Y, Sohrabi H, Vignarajan J, Bourgeat P, Salvado O, et al. Retinal vascular biomarkers for early detection and monitoring of Alzheimer's disease. Transl Psychiatry 2013; 3:e233.
[34] Lim JK, Li QX, He Z, Vingrys AJ, Wong VH, Currier N, et al. The eye as a biomarker for Alzheimer's disease. Front Neurosci 2016; 10:536.
[35] Williams MA, McGowan AJ, Cardwell CR, Cheung CY, Craig D, Passmore P, et al. Retinal microvascular network attenuation in Alzheimer's disease. Alzheimers Dement 2015;1:229–35.
[36] Dougherty G, Varro J. A quantitative index for the measurement of the tortuosity of blood vessels. Med Eng Phys 2000;22:567–74.
[37] Koh V, Cheung CY, Zheng Y, Wong TY, Wong W, Aung T. Relationship of retinal vascular tortuosity with the neuroretinal rim: the singapore malay eye study. Invest Ophthalmol Vis Sci 2010; 51:3736–41.
[38] Koprowski R, Teper SJ, Węglarz B, Wylęgała E, Krejca M, Wróbel Z. Fully automatic algorithm for the analysis of vessels in the angiographic image of the eye fundus. Biomed Eng Online 2012; 11:35.
[39] Owen CG, Rudnicka AR, Mullen R, Barman SA, Monekosso D, Whincup PH, et al. Measuring retinal vessel tortuosity in 10-year-old children: validation of the Computer-Assisted Image Analysis of the Retina (CAIAR) program. Invest Ophthalmol Vis Sci 2009; 50:2004–10.
[40] Ţălu Ş. Characterization of retinal vessel networks in human retinal imagery using quantitative descriptors. Human Veter Med 2013; 5:52–7.
[41] Cheung CY, Zheng Y, Hsu W, Lee ML, Lau QP, Mitchell P, et al. Retinal vascular tortuosity, blood pressure, and cardiovascular risk factors. Ophthalmology 2011;118:812–8.
[42] Gopinath B, Chiha J, Plant AJ, Thiagalingam A, Burlutsky G, Kovoor P, et al. Associations between retinal microvascular structure and the severity and extent of coronary artery disease. Atherosclerosis 2014;236:25–30.
[43] Tsui I, Shamsa K, Perloff JK, Lee E, Wirthlin RS, Schwartz SD. Retinal vascular patterns in adults with cyanotic congenital heart disease. Semin Ophthalmol 2009;24:262–5.
[44] Kanski JJ. In: Kanski JJ, ed. Clinical ophthalmology : a systematic approach. 6th ed. Edinburgh : Elsevier Butterworth-Heinemann; 2007.
[45] Longmuir SQ, Longmuir R, Matthews K, Olson R, Abramoff M. Retinal Arterial but not Venous Tortuosity correlates with Facioscapulohumeral Muscular Dystrophy (FSHD) Severity. Invest Ophthalmol Vis Sci 2009;50:5419.
[46] Ascaso FJ, Cruz N, Modrego PJ, Lopez-Anton R, Santabárbara J, Pascual LF, et al. Retinal alterations in mild cognitive impairment and Alzheimer's disease: an optical coherence tomography study. J Neurol 2014;261:1522–30.
[47] Attems J, Jellinger KA. The overlap between vascular disease and Alzheimer's disease–lessons from pathology. BMC Med 2014;12:206.
[48] Desjardins M, Sylvestre JP, Jafari R, Kulasekara S, Rose K, Trussart R, et al. Preliminary investigation of multispectral retinal tissue oximetry mapping using a hyperspectral retinal camera. Exp Eye Res 2016; 146:330–40.
[49] Optina Diagnostics. [Online]. Available at: http://optinadx.com/. Accessed April 3, 2019.
[50] Patasius M, Marozas V, Jegelevicius D, Lukosevicius A. Evaluation of tortuosity of eye blood vessels using the integral of square of derivative of curvature. In: IFMBE Proc 3rd Eur Med Biol Eng Conf.(EMBEC05); 2005, 11.
[51] Abdalla M, Hunter A, Al-Diri B. Quantifying retinal blood vessels' tortuosity—Review. In: 2015 Science and Information Conference (SAI); 2015. p. 687–93.
[52] Haralick RM, Shanmugam K, Dinstein I. Textural features for image classification. IEEE Trans Syst Man Cybern 1973;SMC-3:610–21.
[53] Brown WR, Thore CR. Review: cerebral microvascular pathology in ageing and neurodegeneration. Neuropathol Appl Neurobiol 2011; 37:56–74.
[54] Cheung CY, Ong YT, Ikram MK, Ong SY, Li X, Hilal S, et al. Microvascular network alterations in the retina of patients with Alzheimer's disease. Alzheimers Dement 2014;10:135–42.
[55] Soucy J-P, Chevrefils C, Sylvestre J-P, Arbour JD, Rhéaume M-A, Beaulieu S, et al. Validation of a hyperspectral retinal imaging method to predict cerebral amyloid PET status. In: 2018 Neuroscience Meeting Planner, San Diego, CA; 2018;14. p. 158.